ISSN 0016-7932, Geomagnetism and Aeronomy, 2016, Vol. 56, No. 8, pp. 1068–1074. © Pleiades Publishing, Ltd., 2016.

Hard X-Ray Generation in the Turbulent Plasma of Solar Flares

Yu. E. Charikov[a, b, *] and A. N. Shabalin[a]

[a] *Ioffe Physical-Technical Institute, Russian Academy of Sciences, St. Petersburg, 194021 Russia*

[b] *Peter the Great St. Petersburg Polytechnic University, St. Petersburg, 195251 Russia*

**e-mail: Y.Charikov@yandex.ru*

Received February 17, 2016; in final form, March 10, 2016

Abstract—The influence of scattering of accelerated electrons in the turbulent plasma on the transformation of their distribution function is studied. The turbulence is connected with the emergence of magnetic inhomogeneities and ion-sound mode. The level of ion-sound turbulence is specified by the ratio $W^s/nk_BT_e = 10^{-3}$, while the value of magnetic fluctuations is $\delta B/B = 10^{-3}$. Different initial angular distributions of the function of accelerated-electron source are regarded: from isotropic to narrow directional distributions. For the chosen energy-density values of the ion-sound turbulence and the level of magnetic fluctuations, it is shown that both types of turbulence lead to a qualitative change in the hard X-ray brightness along the loop, moreover their influence was found to be different. Models with magnetic fluctuations and the ion sound can be distinguished not only by the difference in the hard X-ray distribution along the loop but also by the photon spectrum.

DOI: 10.1134/S0016793216080041

1. INTRODUCTION

As is known, ion-sound waves can only exist if the electron temperature exceeds the ion temperature: $T_e \gg T_i$ (Tsytovich, 1971). Since the time of energy exchange between the electrons and ions in the plasma is inversely proportional to the plasma density, plasma nonisothermality can hold in the upper part of the loop rather than at footpoints. Therefore, the appearance and existence of the ion-sound mode in the magnetic loop should be expected everywhere except footpoints, in which a sharp growth in the density of background plasma is anticipated. These conditions are easily implemented during flares in solar magnetic loops.

Let us briefly discuss possible mechanisms of excitation of ion-sound turbulence. The causes of generation are related to the presence of currents and to the inhomogeneity of magnetic fields in the flare-loop plasma. Both mechanisms may be implemented in flare loops. However, the latter mechanism may hardly be implemented in the most of observed flares, since a sufficiently large field gradient is possible, as a rule, only at footpoints, where the density of background plasma is so high that the process of Coulomb's scattering of electrons dominates. Therefore, the current-related mechanism of ion-sound excitation seems to us to be more probable. The condition for the appearance of such a turbulence is an excess of the electron drift velocity of background plasma over the speed of ion-sound waves, so the Cherenkov excitation of ion-sound turbulence becomes possible. The energy transfer over the spectrum of Langmuir's turbulence can also be a source of ion-sound waves in nonisothermal plasma. Problems of the kinetics of accelerated electrons were solved earlier with allowance for Coulomb's diffusion alone, e.g., in (Hamilton and Petrosian, 1990; Melnikov et al., 2009; Charikov et al., 2012), with accounting for a reverse current (Zharkova, 2010) and with regard for magnetic inhomogeneities (Kontar, 2014; Charikov, 2015). Ion-sound turbulence without consideration of the enumerated effects was discussed in (Kudryavtsev and Charikov, 1991; Brown et al., 1979]. The main difference of this work is the analysis of all indicated effects in the context of particular models of solar magnetic loops.

2. KINETICS OF ACCELERATED ELECTRONS IN FLARE LOOPS

Let us consider a flaring loop as a semicircle. A cross-section of the loop reduces to its footpoints due to magnetic flux conservation. The dynamics of the propagation of a beam of electrons accelerated during the flare is studied on the basis of the solution of the nonstationary relativistic kinetic equation, which takes into account the processes of Coulomb's scattering and magnetic mirroring, the influence of a reverse current, and magnetic turbulence in magnetic configurations with the specified distribution of plasma density and magnetic field induction. A distinctive feature

of this work is the consideration of the influence of ion-sound oscillations in the plasma on the electron distribution function.

We write the kinetic equation in the form (its particular terms can be found in (Hamilton and Petrosian, 1990; Zharkova, 2010; Kontar, 2014; Kudryavtsev and Charikov, 1991)

$$\frac{\partial f}{\partial t} = -c\beta\mu\frac{\partial f}{\partial s} + c\beta\frac{\partial \ln(B)}{\partial s}\frac{\partial}{\partial \mu}\left[\frac{\left(1-\mu^2\right)}{2}f\right] + C_1\frac{c}{\lambda_0}\frac{\partial}{\partial E}\left(\frac{f}{\beta}\right) + C_2\frac{c}{\lambda_0\beta^3\gamma^2}\frac{\partial}{\partial \mu}\left[\left(1-\mu^2\right)\frac{\partial f}{\partial \mu}\right] + \frac{eE^*\beta\mu}{m_e c}\frac{\partial f}{\partial E} + \frac{eE^*(1-\mu^2)}{m_e\beta c}\frac{\partial f}{\partial \mu} + D^s\frac{\partial}{\partial \mu}\left[\left(1-\mu^2\right)\frac{\partial f}{\partial \mu}\right] + \left(\frac{\delta B}{B}\right)^2\frac{c\beta}{2\lambda_B}\frac{\partial}{\partial \mu}\left[|\mu|\left(1-\mu^2\right)\frac{\partial f}{\partial \mu}\right] + S(E,\mu,s,t), \quad (1)$$

where $f(E, \mu, s, t)$ is the accelerated-electron distribution function, s is the distance along the magnetic field line (counted from the loop top), t is the running time, $\mu = \cos\alpha$ is the cosine of a pitch angle, $\lambda_0(s) = \frac{10^{24}}{n(s)\ln\Lambda}$ cm, $n(s)$ is plasma density, $\ln\Lambda$ is Coulomb logarithm, $\beta = v/c$, v is the velocity of accelerated electrons, c is the speed of light, $\gamma = E + 1$ is the Lorenz factor of an electron, E is the kinetic energy of an electron expressed in units of the electron's rest mass energy, λ_B is the characteristic longitudinal correlation length of magnetic field fluctuations, $C_1 = x + \frac{1-x}{2}\frac{\ln\beta^2\gamma^2 E/\alpha_F^4}{\ln\Lambda}$, $C_2 = \frac{1}{2} + \frac{1+\gamma}{4}C_1$, α_F is the fine structure constant, x is the fraction of ionized hydrogen atoms, D^s is the diffusion coefficient for the ion sound $D^s = \left(\frac{v/v_{is}}{m_e\beta c}\right)D_l$, $D_l = \frac{15\sqrt{\pi}}{8\sqrt{2}}Z^2 m_e^2 v_{T_e}^5\left(\frac{m_e}{m_i}\right)^{\frac{3}{2}} \times \frac{T_e}{T_i}k_g v_{T_e}\left(\frac{1}{2Ec^2}\right)^{\frac{3}{2}}\left[\sqrt{\frac{Q}{Q_*^S}} + e^{-\sqrt{\frac{Q}{Q_*^S}}} - 1\right]$, $\frac{Q}{Q_*^S} = \frac{T_i}{T_e}\sqrt{\frac{m_i}{m_e}}\frac{W^s}{nk_B T_e}$, T_i and T_e are the temperatures of the ionic and electronic plasma components (Tsytovich, 1971). In this work, a stationary level of ion-sound turbulence is suggested $W^s/nk_B T_e = 10^{-3}$. This value corresponds with the still weak turbulence. With smaller values, scattering on the ion sound is not efficient in comparison with Coulomb's scattering. The generation of the ion-sound mode is possible when the accelerated electron stream propagates along the magnetic loop and a reverse compensating current arises, which is caused by the induced electric field

$$E^*(s,t) = \frac{j(s,t)}{\sigma(s)} = \frac{e}{\sigma(s)} \times \int_{E_{min}}^{E_{max}} v(E)dE\int_{-1}^{1} f(E,\mu,s,t)\mu d\mu,$$

$\sigma(s)$ is the conductivity of background plasma. It should be noted that the turbulent diffusion coefficient $D_{\mu\mu}^T$ is defined by the form of the spectrum of magnetic field fluctuations or the correlation function, which are unknown for solar flares at the present time (Lee, 1982).

The plasma density distribution along the loop is specified phenomenologically on the basis of RHESSI observations in the region of chromosphere $n_e = 1.25\times10^{13}\left(z/1\text{Mm}\right)^{-2.5}\text{cm}^{-3}$, where z is the height (Aschwanden, 2002). The issue of magnetic field distribution in the loop is even more uncertain; the only criterion for its specification is the convergence of the field induction to the loop footpoints. In previous works, e.g., (Hamilton et al., 1990; Melnikov et al., 2009; Zharkova et al., 2010; Charikov et al., 2012), only the longitudinal component of the magnetic field induction directed along the s axis, which depends on the s coordinate, was taken into account. We will specify the modeled magnetic field that converges to the loop footpoints in accordance with (McClements, 1992) in the form $\frac{B(s)}{B_0} = 1 + \frac{(s-b_1)^2}{h_b^2}$, where $B_0 = 200$ G is a minimum value of the magnetic field, while b_1 specifies the spatial displacement of the magnetic field minimum from the geometric apex of the loop. The ratio B_{max}/B_0 varied (assumed to be 2 in the majority of models). The value of the characteristic scale of a change in the magnetic field h_b is determined on the basis of the specified ratio B_{max}/B_0 and the quantity b_1. At the moment of injection, the functional dependence of the accelerated-electron source on arguments is presented in factorized form, i.e., independence is believed to exist for the processes that lead to forming such a distribution function during the electron acceleration: $S(E,\alpha,s,t) = KS_1(E)S_2(\alpha)S_3(s)S_4(t)$, where K is the normalization factor which is fitted on the basis of the specified energy flux of accelerated electrons: $K = 2.1 \times 10^{-3}$ cm^{-3} s^{-1} for an isotropic source and $K = 2.7 \times 10^{-2}$ cm^{-3} s^{-1} for an anisotropic source. The energy fluxes used vary within a range of 10^{10}–10^{11} erg cm^{-2} s^{-1}. The electron energy spectrum in the source is a power-law with the spectral index δ. Cases of isotropic injection $S_2(\alpha) = 1$ and anisotropic distribution of electrons along the magnetic field within the certain cone of pitch angles $S_2(\alpha) = \cos^{12}(\alpha)$ are considered. The choice of an exponent equal to 12 is associated with the need to calculate the

maximally anisotropic source with which the numerical calculation still remains stable. An injection of accelerated electrons occurs in the upper part of the loop. The temporal profile at the moment of injection is an individual pulse in the form of a Gaussian with a characteristic pulse width of 1.4 s.

The hard X-ray (HXR) intensity is calculated according to formulas of relativistic bremsstrahlung (Gluckstern and Hull, 1953; Bai and Ramaty, 1978). Unlike many previous works on HXR calculation (see (Aschwanden, 2002) and references therein), we take into account the real position of the magnetic loop on the solar disk, which implies the calculation of HXR flux at each point of the loop at local angle of observation, as well as the regard for geometric volume of the loop. For model calculations, the loop cross-section is a semicircle with a center located at the distance of 955 arcsec from the Sun disk center along the horizontal heliocentric axis and 0 arcsec along the vertical axis.

3. INFLUENCE OF ION-SOUND TURBULENCE AND MAGNETIC FLUCTUATIONS ON HXR BRIGHTNESS DISTRIBUTION

Let us consider the results of X-ray bremsstrahlung along the flare loops. The injection of accelerated electrons occurred in the vicinity of looptop. The magnetic field induction is believed to be 200 G at the looptop and 400 G at footpoints. The index of the power-law spectrum of accelerated electrons is $\delta = 5$. First, we will discuss the results for an isotropic model of electron injection. Figure 1 presents results of HXR flux calculation for the energies $\varepsilon_x = 29–58$ keV and $\varepsilon_x = 70–135$ keV (panels a and b, respectively) and the accelerated-electron distribution functions for different models (panels c–h) at the peak time $t = 2.6$ s. The panels on the left (c, e) display the calculation results for one footpoint of the magnetic loop, while the panels on the right (d, f) show the results for the looptop. We will consider in detail the nature of changes in the HXR and distribution functions for different models depending on the distance along the loop and the pitch angle of electrons. Curve *1* corresponds to the model in which the processes of scattering on magnetic fluctuations and ion-sound turbulence are disregarded. Distributions over the pitch angle for the 30-keV electrons show that the quasi-transverse distribution forms at the looptop in this model (panel d), whereas the electron distribution at the loop footpoint is closer to the longitudinal distribution (panel c). Similar distributions were obtained earlier (Charikov et al., 2012). In this work, we consider additional mechanisms of electron scattering on magnetic field inhomogeneities or on ion-sound waves. Curve *2* on these panels correspond to the model with allowance for magnetic inhomogeneities with the level $\delta B/B = 10^{-3}$. Curve *3* shows the results from calculation with accounting of the scattering on ion-sound turbulence with the level $W^s/nk_BT_e = 10^{-3}$. Finally, model 4 considers both possibilities. We note especially that electron distributions over pitch angles at the looptop change their shape and become isotropic (Figs. 1d, 1f). This change in distributions is easily explained by the effective additional scattering of electrons. Moreover, the low-energy electrons are scattered most efficiently (compare the distributions in Figs. 1c and 1e and Figs. 1d and 1f). We will note the more efficient scattering of electrons by the ion-sound mode as compared with scattering on inhomogeneities of the magnetic field. A distribution of electrons along the magnetic loop is presented on Figs. 1g and 1h for the energies $E = 30$ keV and $E = 192.2$ keV. The accumulation of electrons, primarily low-energy electrons, at the looptop can be noted, especially with allowance for scattering on ion-sound turbulence. In the presence of magnetic fluctuations, the particle path reduces as energy grows, which is caused by an increase in the Larmor radius and by particle scattering due to inhomogeneities of increasing scale (the energy density spectrum of fluctuations grows as the wave vector **k** reduces). As a result, energetic particles are scattered and captured more efficiently, which can be seen in a comparison of curves *1* and *2* in Figs. 1g and 1h, with accumulation occurring in the legs. When only the ion sound is taken into consideration (model 3, Fig. 1a), the strong HXR source at the looptop appears, in contrast to model 2. The ion-sound turbulence scatters the low-energy electrons more effectively. As a result, a significant number of electrons is accumulated at the looptop. Some low-energy electrons leaving the looptop, due to the change from the quasi-transverse electron distribution to the isotropic distribution as a result of scattering on the ion-sound turbulence (see curves *1* and *3* in Figs. 1d and 1f), are captured again in the leg. The efficiency of particle capture can be assessed by Fig. 2, in which the fluxes of electrons along the loop up and down are separated. In Fig. 2a, it can be seen that ratios of up and down fluxes are roughly the same for models 1 and 2 in legs. In model 3 with the ion sound, the number of electrons propagating in the opposite direction, toward the looptop, is equal to the number of electrons flying toward the loop footpoints (see Fig. 2b). The efficiency of electron scattering on magnetic fluctuations as compared with the efficiency of scattering on the ion-sound turbulence, depending on energy, can be assessed from curves *4* and *3* in Figs. 1a–1h (curve *4* is a combined model in which magnetic fluctuations and ion-sound turbulence are taken into account). As is evident, only in the case of high energies of electrons does the influence of magnetic fluctuations become noticeable (see curves *4* and *3* in Fig. 1h).

Since a contribution to the radiation in the energy range of 29–58 keV is made also by the higher-energy electrons, the effect of scattering of the higher-energy

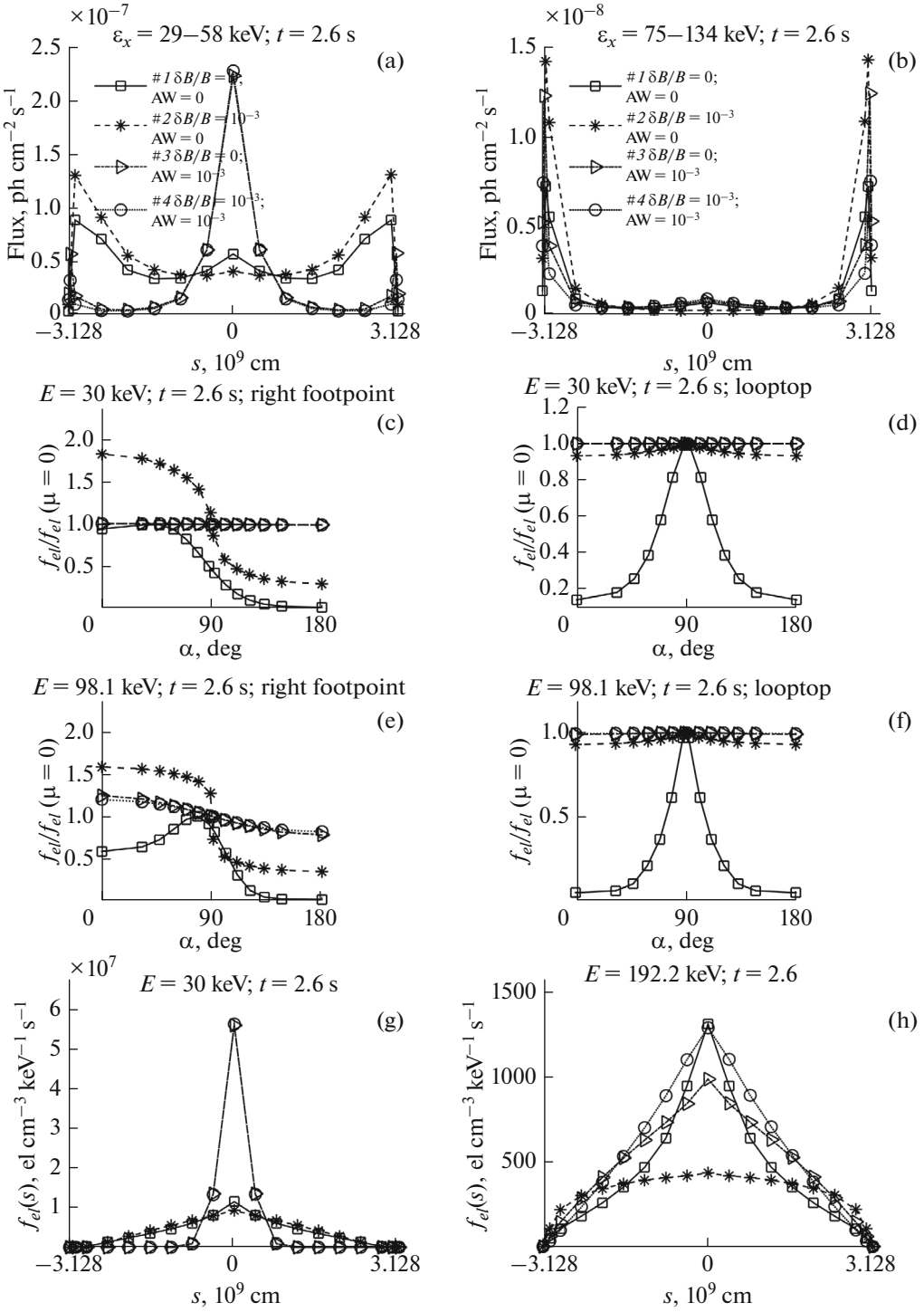

Fig. 1. (a, b) HXR distribution, integrated with respect to cross section, in the energy ranges of (a) $\varepsilon_x = 29–58$ keV, (b) $\varepsilon_x = 70–135$ keV. Curves *1–4* show results for cases when (*1*) the magnetic and ion-sound turbulences are absent, (*2*) the magnetic turbulence is distributed homogeneously along the loop, (*3*) the ion-sound turbulence is distributed homogeneously along the loop, (*4*) the magnetic and ion-sound turbulences are distributed homogeneously along the loop. (c, d) Angular dependence of the energy-differential electron distribution function integrated over the sufficiently wide loop region (c) at the footpoint and (d) at the looptop for the electron energy $E = 30$ keV. (e, f) The same as on panels (c) and (d) but for the energy $E = 98.1$ keV. The electron distribution function is normalized to its value at the pitch angle $\alpha = 90°$. (g, h) Functions of electron distribution along the loop for energy values of (g) $E = 30$ keV and (h) $E = 192.2$ keV. The descriptions of curves on panels (c, d, e, f, g, h) coincide with those for panels (a) and (b). The source of electrons is isotropic: $S(\alpha) = 1$. The plot corresponds to the time instant of the injection maximum. The designation $AW = W^s / nk_B T_e = 10^{-3}$ in the figure relates to the models with allowance for the ion-sound turbulence.

electrons on magnetic fluctuations has an impact on the radiation in the energy range of 29–58 keV. At low quanta energies of 29–58 keV, a bright HXR source forms in the region, closer to the loop footpoints. The emission from footpoints at 29–58 keV is suppressed when the ion sound is taken into account. While in the range of photon energies of 70–134 keV, the footpoint brightness considerably exceeds the brightness of sources at the looptop (see Fig. 1b). In this case, the ion-sound turbulence does not exert a strong influence on the HXR source at the looptop.

Figure 3 shows the results of similar calculations for the anisotropic electron source with a narrow distribution over the pitch angle at the moment of ejection: $S(\alpha) = \cos^{12}(\alpha)$. The index of electron spectrum is $\delta = 5$. Curve *1* corresponds to the model without turbulence, curve *2* relates to the model with magnetic fluctuations, and curve *3* applies to the model with the ion-sound turbulence. The results of the calculation of the function of accelerated-electron distribution over pitch angles for two energies (30 and 98 keV) are presented in Figs. 2c and 2d and Figs. 2e and 2f, respectively. As is evident, the regard for scattering on magnetic fluctuations and ion-sound oscillations has changed the nature of the electron distribution function, both at the looptop and at footpoints. For example, for the 30-keV electrons, the anisotropic distribution changed to isotropic distribution. For the higher-energy electrons with the 98-keV energy (Fig. 3e), the account of the additional scattering leads to an increase in the backscattered electrons, i.e., electrons with pitch angles of more than 90°. Let us consider the HXR distributions along the magnetic loop corresponding to the peak of electron injection during the flare. In Fig. 3a, the similar distributions of X-rays with energies in a range of 29–58 keV are shown for three models. Since the flux of accelerated electrons is symmetrical with respect to the looptop, the HXR flux also has a symmetric distribution. A comparison of HXR distributions for the cases of isotropic and anisotropic injection models reveals their qualitative coincidence (except model 1, without turbulence). In the anisotropic case a HXR source that is brighter relative to the loop footpoints formed in model 2 with magnetic fluctuations at the looptop. It differs from isotropic case (see Fig. 1a, model 2 in comparison with model 1), what is caused by the initial quasi-longitudinal distribution of electrons (see Figs. 3d, 3f). It changes into the isotropic distribution, which leads to the enhanced accumulation of electrons in the entire loop (see Figs. 3g, 3h). The ion-sound turbulence (curve *3*, Fig. 3a) exerts a more effective impact on electron scattering in pitch angles, which results in a very bright looptop and the brightness decrease in footpoints (see Fig. 3g). Thus, the presence of the ion-sound turbulence with a level $W^s/nk_BT_e = 10^{-3}$, even in the case of the strongly anisotropic source, leads to the fully isotropic electrons responsible for radiation in the range of up to 60 keV (see Figs. 3c–3f).

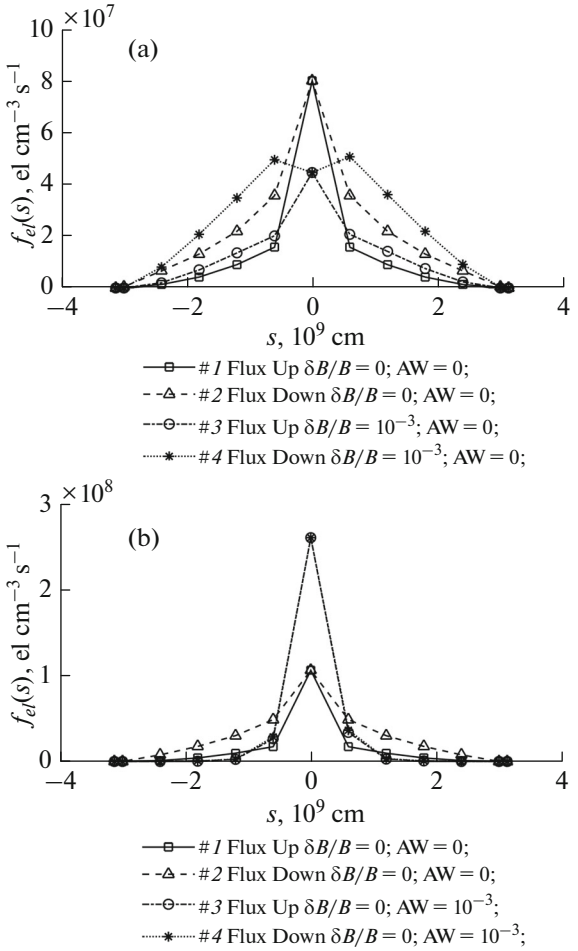

Fig. 2. Electron distribution functions (integrated over all energies) along the loop. The integration with respect to angles is partial and performed in such a way that fluxes of electrons flying up and down are separated. (a) Curves *1*, *2* correspond to the fluxes up and down, respectively, for model 1; curves *3* and *4* relate to the fluxes up and down, respectively, for model 2 (i.e., with magnetic fluctuations). (b) Curves *1* and *2* are the same as on panel a, while curves *3* and *4* correspond to model 3 (i.e., with ion sound). The source of electrons is isotropic: $S(\alpha) = 1$. The plot corresponds to the time instant of the injection maximum. The designation $AW = W^s/nk_BT_e = 10^{-3}$ in the figure relates to the models taking into account the ion-sound turbulence.

4. CONCLUSIONS

In this work, the influence of magnetic fluctuations and ion-sound turbulence on the transfer of accelerated electrons in the solar flare loop was analyzed. For the chosen energy-density levels of turbulence in the case of magnetic fluctuations $\delta B/B = 10^{-3}$ and in the case of ion sound $W^s/nk_BT_e = 10^{-3}$, it was shown that, when the source of electrons is isotropic, both types of turbulence lead to a qualitative change in

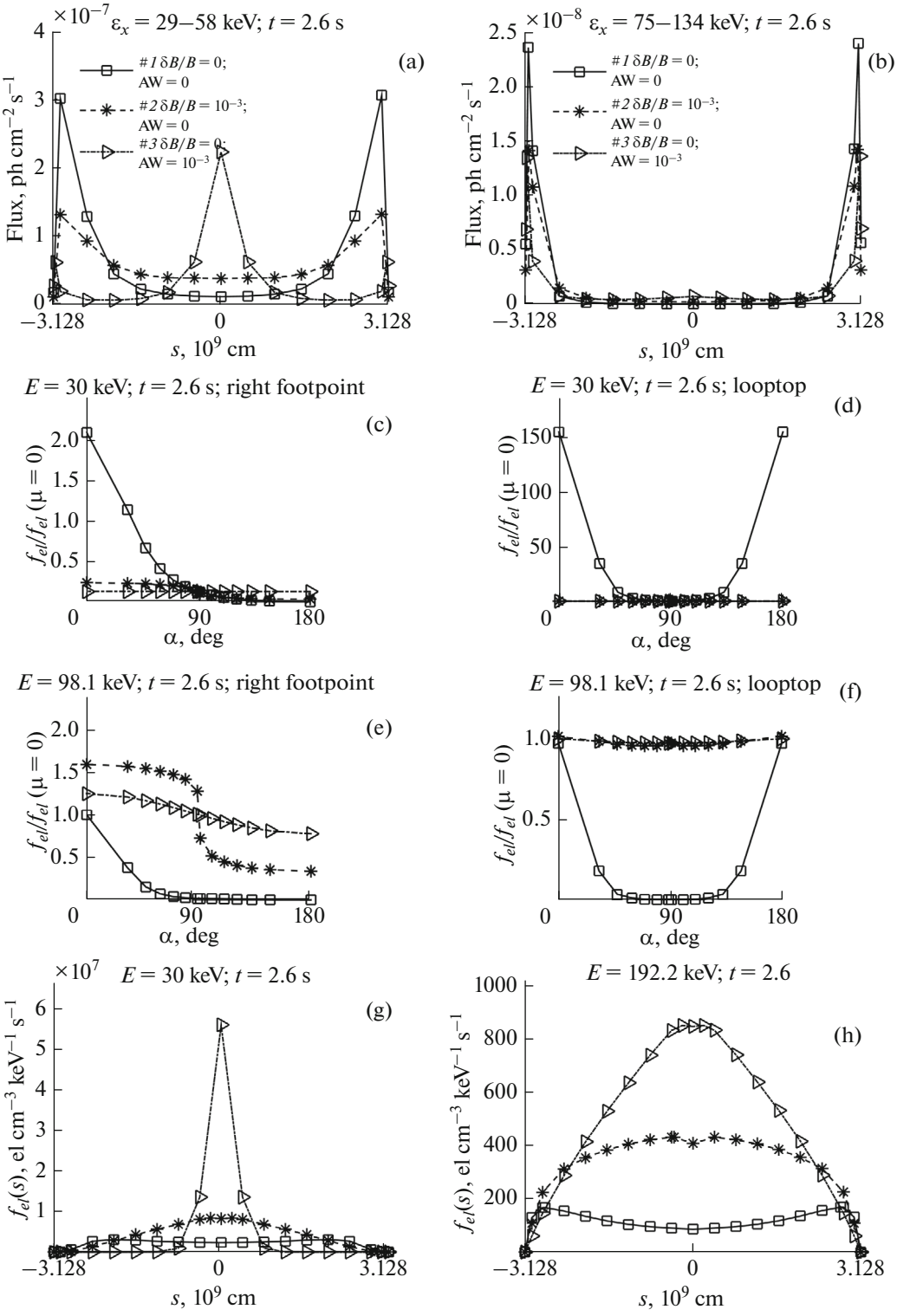

Fig. 3. The same as in Fig. 1 but for the case of the anisotropic injection of electrons: $S(\alpha) = \cos^{12}(\alpha)$.

the HXR distribution along the loop. Moreover, the impact of these turbulence types proves to be different. Electrons are scattered most effectively on ion-sound waves. It was also shown that the effects can differ qualitatively for the case of various anisotropy of the electrons. For example, magnetic fluctuations for the isotropic source $S(\alpha) = 1$ lead to attenuation of the emission from the looptop and, in contrast, to its

enhancement in the case of $S(\alpha) = \cos^{12}(\alpha)$. It was also demonstrated that, with identical suggestions relative to the spectral density of energy, the ion-sound turbulence proves to be much more efficient in estimating the influence on the 29–58 keV emission, even though the density of magnetic energy under conditions of flare loops is many times larger than the energy density of the background plasma.

ACKNOWLEDGMENTS

The work of A.N. Shabalin was partly supported by the Russian Foundation for Basic Research (project no. 14-02-00924) and by the Fundamental Research Program no. 7 of the Presidium of the Russian Academy of Sciences.

REFERENCES

Aschwanden, M.J., Brown, J.C., and Kontar, E.P., Chromospheric height and density measurements in a solar flare observed with RHESSI. II. Data analysis, *Sol. Phys.*, 2002, vol. 210, pp. 383–405.

Bai, T. and Ramaty, R., Backscatter, anisotropy, and polarization of solar hard X-rays, *Astrophys. J.*, 1978, vol. 219, pp. 705–726.

Brown, J.C., Spicer, D.S., and Melrose, D.B., Production of a collisionless conduction front by rapid coronal heating and its role in solar hard X-ray bursts, *Astrophys. J.*, 1979, vol. 228, pp. 592–597.

Charikov, Yu.E., Melnikov, V.F., and Kudryavtsev, I.V., Intensity and polarization of the hard X-ray radiation of solar flares at the top and footpoints of a magnetic loop, *Geomagn. Aeron. (Engl. Transl.)*, 2012, vol. 52, no. 8, pp. 1021–1031.

Charikov, Yu.E. and Shabalin, A.N., Influence of magnetic turbulence on the propagation of accelerated electrons and hard X-ray brightness distribution in solar flares, *Geomagn. Aeron. (Engl. Transl.)*, 2015, vol. 55, no. 8, pp. 1104–1111.

Gluckstern, R.L. and Hull, M.H., Polarization dependence of the integrated bremsstrahlung cross section, *Phys. Rev.*, 1953, vol. 90, no. 6, pp. 1030–1035.

Hamilton, R.J., Lu, E.T., and Petrosian, V., Numerical solution of the time-dependent kinetic equation for electrons in magnetized plasma, *Astrophys. J.*, 1990, vol. 354, pp. 726–734.

Kontar, E.P., Bian, N.H., Emslie, A.G., and Vilmer, N., Turbulent pitch-angle scattering and diffusive transport of hard-X-ray producing electrons in flaring coronal loops, *Astrophys. J.*, 2014, vol. 780, no. 2, id 176.

Kudryavtsev, I.V. and Charikov, Yu.E., Kinetics of fast electrons in ion-acoustic waves in the turbulent plasma of solar flares, *Astron. Zh.*, 1991, vol. 68, nos. 4–6, pp. 825–836.

Lee, M.A., Coupled hydromagnetic wave excitation and ion acceleration upstream of the Earth's bow shock, *J. Geophys. Res.*, 1982, vol. 87, no. A7, pp. 5063–5080.

McClements, K.G., The simultaneous effects of collisions, reverse currents and magnetic trapping on the temporal evolution of energetic electrons in a flaring coronal loop, *Astron. Astrophys.*, 1992, vol. 258, pp. 542–548.

Melnikov, V.F., Gorbikov, S.P., and Pyatakov, N.P., Formation of anisotropic distributions of mildly relativistic electrons in flaring loops, *Symp. – Int. Astron. Union*, 2009, vol. 257, pp. 323–328.

Tsytovich, V.N., *Teoriya turbulentnoi plazmy* (Theory of Turbulent Plasma), Moscow: Atomizdat, 1971.

Zharkova, V.V., Kuznetsov, A.A., and Siversky, T.V., Diagnostics of energetic electrons with anisotropic distributions in solar flares. I. Hard X-rays bremsstrahlung emission, *Astron. Astrophys.*, 2010, vol. 512, id A8.

Translated by M. Samokhina